

SAMPLET BASIS PURSUIT: MULTIREOLUTION SCATTERED DATA APPROXIMATION WITH SPARSITY CONSTRAINTS

DAVIDE BAROLI, HELMUT HARBRECHT, AND MICHAEL MULTERER

ABSTRACT. We consider scattered data approximation in samplet coordinates with ℓ_1 -regularization. The application of an ℓ_1 -regularization term enforces sparsity of the coefficients with respect to the samplet basis. Samples are wavelet-type signed measures, which are tailored to scattered data. They provide similar properties as wavelets in terms of localization, multiresolution analysis, and data compression. By using the Riesz isometry, we embed samples into reproducing kernel Hilbert spaces and discuss the properties of the resulting functions. We argue that the class of signals that are sparse with respect to the embedded samplet basis is considerably larger than the class of signals that are sparse with respect to the basis of kernel translates. Vice versa, every signal that is a linear combination of only a few kernel translates is sparse in samplet coordinates. Therefore, samples enable the use of well-established multiresolution techniques on general scattered data sets.

We propose the rapid solution of the problem under consideration by combining soft-shrinkage with the semi-smooth Newton method. Leveraging on the sparse representation of kernel matrices in samplet coordinates, this approach converges faster than the fast iterative shrinkage thresholding algorithm and is feasible for large-scale data. Numerical benchmarks are presented and demonstrate the superiority of the multiresolution approach over the single-scale approach. As large-scale applications, the surface reconstruction from scattered data and the reconstruction of scattered temperature data using a dictionary of multiple kernels are considered.

1. INTRODUCTION

Sparsity constraints have a wide applicability in machine learning, statistics, as well as in signal processing. Examples for the latter are deblurring, feature selection and compressive sensing, see [4, 7, 12, 23, 31]. In practice, sparsity constraints are imposed by adding an ℓ^1 -regularization term to the objective function. However, sparsity constraints only make sense if a basis is used for the representation where the data actually becomes sparse. In the past, mostly wavelet bases, Fourier bases, or frames like curvelets, contourlets, and shearlets have been used as they are known to give rise to sparse representations, see [5, 10, 11, 14, 17] for instance. However, such discretization concepts are based on regular grids and it is not obvious how to extend them to scattered data as they typically appear in applications.

In the present article, we employ *samples* for imposing sparsity. Samples have been invented in [19] and extend the concept of multiresolution analyses and respective wavelet bases to scattered data. The construction relies on the idea of Tausch and White [32], who defined orthonormal multiresolution bases with vanishing moments bottom-up by employing a hierarchical cluster tree. Indeed, as shown in [19], samplet expansions of smooth functions are sparse, allowing for data compression and singularity extraction [26]. As a consequence, kernel matrices issuing from asymptotically smooth kernels can be compressed in samplet representation to very sparse matrices. According to [20], such samplet compressed kernel matrices form a sparse matrix algebra, enabling efficient scattered data analysis.

In this article, we consider scattered data approximation, which is known to be an ill-posed but uniquely solvable problem, see [13, 34] for instance. By means of the Riesz isometry, we embed samples into reproducing kernel Hilbert spaces and examine the properties of the resulting Riesz representers. Then, every signal that is a linear combination of only a few kernel translates is sparse in samplet coordinates. However, the class of signals that are sparse with respect to the samples' Riesz representers is much larger than the class of signals that are sparse with respect to the basis of kernel translates. Thus, in view of the hierarchical structure of the samplet basis, well-established multiresolution techniques become applicable on general scattered data sets.

To enforce the sparsity, we apply regularization with respect to the ℓ^1 -norm, which improves the feature selection in comparison with the standard Tikhonov regularization. Dealing with such *sparsity constraints* in an

efficient way is also mandatory for *basis pursuit*, that is, for decomposing given data into an optimal superposition of dictionary elements, where optimal means having the smallest ℓ^1 -norm of coefficients among all such decompositions, see [8, 27, 33] for instance. We demonstrate that basis pursuit problem can efficiently be solved by using a samplet basis. In particular, the samplet representation we obtain is extremely sparse.

In literature, the ℓ^1 -regularization term is treated numerically by using the iterative shrinkage-thresholding algorithm (ISTA), see [10], and its accelerated counterpart which is the fast iterative-shrinkage thresholding algorithm (FISTA), see [1]. Another approach to solve the underlying optimization problem is the alternating direction method of multipliers (ADMM), see [3], which we however do not consider here. Instead, we follow the idea of [15] and apply the semi-smooth Newton method, which corresponds to an active set method, cp. [9, 22]. As we will see, this leads to an efficient solver for the problem under consideration. Extensive numerical tests are presented and validate the feasibility and power of the proposed approach. Our benchmarks demonstrate the superiority of the multiresolution approach over the single-scale approach. As large-scale applications, we consider the surface reconstruction from noisy measurement data and the reconstruction of temperature data using a dictionary of multiple kernels.

The rest of this article is structured as follows. In Section 2, we introduce reproducing kernel Hilbert spaces and the scattered data approximation problem. Then, in Section 3, we recapitulate the concept of samplets and introduce their embedding into reproducing kernel Hilbert spaces by means of the Riesz isometry. In particular, we discuss the properties of the dual basis and its role in the sparse representation of scattered data. Section 4 starts from traditional kernel ridge regression and then presents scattered data approximation with sparsity constraints in samplet coordinates. We call the resulting approach samplet basis pursuit which especially allows for the usage of a dictionary of several kernels. Solution algorithms to compute sparse samplet expansions, particularly suited for large-scale data, are proposed in Section 5. Extensive numerical tests are presented in Section 6. Finally, in Section 7, we draw the conclusion of the article.

2. PROBLEM FORMULATION

Let $(\mathcal{H}, \langle \cdot, \cdot \rangle_{\mathcal{H}})$ be a Hilbert space of functions $h: \Omega \rightarrow \mathbb{R}$ for some set $\Omega \subset \mathbb{R}^d$. Furthermore, let \mathcal{K} be a continuous, symmetric, and positive definite kernel, i.e., for any set $X := \{\mathbf{x}_1, \dots, \mathbf{x}_N\} \subset \Omega$ of mutually distinct points, the *kernel matrix*

$$(1) \quad \mathbf{K} := [\mathcal{K}(\mathbf{x}_i, \mathbf{x}_j)]_{i,j=1}^N \in \mathbb{R}^{N \times N}$$

is symmetric and positive definite. The kernel \mathcal{K} is the reproducing kernel of \mathcal{H} , iff $\mathcal{K}(\mathbf{x}, \cdot) \in \mathcal{H}$ for every $\mathbf{x} \in \Omega$ and $h(\mathbf{x}) = \langle \mathcal{K}(\mathbf{x}, \cdot), h \rangle_{\mathcal{H}}$ for every $h \in \mathcal{H}$. In this case, we call $(\mathcal{H}, \langle \cdot, \cdot \rangle_{\mathcal{H}})$ a *reproducing kernel Hilbert space*.

For a continuous function $f \in C(\Omega)$, we shall use the notation

$$(f, \delta_{\mathbf{x}})_{\Omega} := \delta_{\mathbf{x}}(f) = f(\mathbf{x}), \quad \mathbf{x} \in \Omega,$$

for the point evaluation, i.e., $\delta_{\mathbf{x}} \in [C(\Omega)]'$ is the point evaluation functional at $\mathbf{x} \in \Omega$. Since the kernel $\mathcal{K}(\mathbf{x}, \cdot)$ is the Riesz representer of the point evaluation $(\cdot, \delta_{\mathbf{x}})_{\Omega}$, we particularly have

$$(2) \quad (h, \delta_{\mathbf{x}})_{\Omega} = \langle \mathcal{K}(\mathbf{x}, \cdot), h \rangle_{\mathcal{H}} \quad \text{for every } h \in \mathcal{H}.$$

Given the set $X = \{\mathbf{x}_1, \dots, \mathbf{x}_N\} \subset \Omega$, we introduce the subspace

$$(3) \quad \begin{aligned} \mathcal{H}_X &:= \text{span}\{\phi_1, \dots, \phi_N\} \subset \mathcal{H}, \\ \phi_i &:= \mathcal{K}(\mathbf{x}_i, \cdot) \text{ for } i = 1, \dots, N. \end{aligned}$$

We call the basis ϕ_1, \dots, ϕ_N of \mathcal{H}_X the *basis of kernel translates*.

The subspace \mathcal{H}_X is isometrically isomorphic to the subspace $\mathcal{X} := \text{span}\{\delta_{\mathbf{x}_1}, \dots, \delta_{\mathbf{x}_N}\} \subset \mathcal{H}'$ by means of the Riesz isometry. We may thus identify

$$u' = \sum_{i=1}^N u_i \delta_{\mathbf{x}_i} \in \mathcal{X} \quad \text{with} \quad u = \sum_{i=1}^N u_i \mathcal{K}(\mathbf{x}_i, \cdot) \in \mathcal{H}_X.$$

To provide a notion of orthogonality in \mathcal{X} , we introduce the inner product

$$\langle u', v' \rangle_{\mathcal{X}} := \sum_{i=1}^N u_i v_i, \quad u' = \sum_{i=1}^N u_i \delta_{\mathbf{x}_i}, \quad v' = \sum_{i=1}^N v_i \delta_{\mathbf{x}_i}.$$

We remark that this inner product differs from the restriction of the canonical one in \mathcal{H} to \mathcal{H}_X . The latter is given by

$$\langle u, v \rangle_{\mathcal{H}} = \mathbf{u}^\top \mathbf{K} \mathbf{v}$$

with the kernel matrix \mathbf{K} from (1), and the coefficient vectors $\mathbf{u} := [u_i]_{i=1}^N$, $\mathbf{v} := [v_i]_{i=1}^N$.

A direct consequence of the duality between \mathcal{H}_X and \mathcal{X} is that the \mathcal{H} -orthogonal projection of a function $h \in \mathcal{H}$ onto \mathcal{H}_X is given by the interpolant

$$s_h := \sum_{i=1}^N \alpha_i \mathcal{K}(\mathbf{x}_i, \cdot),$$

which satisfies

$$(4) \quad s_h(\mathbf{x}_i) = h(\mathbf{x}_i) \quad \text{for all } \mathbf{x}_i \in X.$$

In other words, the interpolation problem (4) corresponds to a Galerkin formulation for the \mathcal{H} -orthogonal projection onto \mathcal{H}_X . There holds (4), iff

$$(5) \quad \langle s_h, v \rangle_{\mathcal{H}} = \langle h, v \rangle_{\mathcal{H}} \quad \text{for all } v \in \mathcal{H}_X.$$

Choosing the basis of kernel translates $\phi_i = \mathcal{K}(\mathbf{x}_i, \cdot)$ as ansatz- and test functions in (5), the expansion coefficients

$$\boldsymbol{\alpha} := [\alpha_i]_{i=1}^N$$

can be retrieved by solving the linear system

$$(6) \quad \mathbf{K} \boldsymbol{\alpha} = \mathbf{h}, \quad \mathbf{h} := [h(\mathbf{x}_i)]_{i=1}^N.$$

Depending on the choice of the kernel function, the linear system (6) is typically ill-conditioned and a suitable regularization is required to obtain a solution. Within this article, our focus is on ℓ^1 -regularization with respect to an appropriate multiresolution analysis. The corresponding multiresolution basis is introduced in the next section.

3. SAMPLETS

3.1. Samplet bases. We equip the space $\mathcal{X} \subset \mathcal{H}'$ with a multiresolution analysis

$$\mathcal{S}_j = \text{span}\{\sigma_{j,k}\}_k, \quad j = 0, \dots, J,$$

whose basis elements are called *samplets*, such that

$$\mathcal{X} = \mathcal{X}_J = \bigoplus_{j=0}^J \mathcal{S}_j \quad \text{and} \quad \mathcal{S}_\ell \perp \mathcal{S}_j \text{ for } \ell \neq j.$$

Each samplet has a representation with respect to the point evaluation functionals in \mathcal{X} , i.e.,

$$(7) \quad \sigma_{j,k} = \sum_{i=1}^n \omega_{j,k,i} \delta_{\mathbf{x}_i}.$$

For the expansion coefficients, we introduce the coefficient vectors $\boldsymbol{\omega}_{j,k} = [\omega_{j,k,i}]_i$. In view of (7), samplets can be defined on arbitrary scattered data sets. In particular, the samplet basis can be constructed in linear time with respect to the number of points N in a black-box fashion and in arbitrary dimension. In this regard, they overcome well known limitations of wavelets, which are usually constructed only in one spatial dimension on equispaced data sets. For all the details on the construction samplets, we refer to [19].

The properties of samplets are summarized by the following theorem, which is a compilation of results from [18, 19, 32] for cardinality balanced hierarchical cluster trees for X . Note that the *support* $\nu_{j,k}$ of a samplet $\sigma_{j,k}$ is to be understood as the smallest convex set which contains all points with non-vanishing samplet coefficients.

Theorem 3.1. *The samplet basis $\bigcup_{j=0}^J \{\sigma_{j,k}\}_k$ forms an orthonormal basis in \mathcal{X} , satisfying the following properties:*

- (1) *There holds $c^{-1}2^j \leq \dim \mathcal{S}_j \leq c2^j$ for a constant $1 < c \leq 2$.*
- (2) *The samplets have vanishing moments of order $q + 1$, i.e., $(p, \sigma_{j,k})_\Omega = 0$ for all $p \in \mathcal{P}_q(\Omega)$, where $\mathcal{P}_q(\Omega)$ is the space of polynomials up to degree q .*
- (3) *The coefficient vector $\boldsymbol{\omega}_{j,k} = [\omega_{j,k,i}]_i$ of the samplet $\sigma_{j,k}$ satisfies $\|\boldsymbol{\omega}_{j,k}\|_1 \leq c2^{(J-j)/2}$ for a constant $0 < c < 2$.*
- (4) *Given $f \in C^{q+1}(\nu_{j,k})$, there holds*

$$\begin{aligned} & |(f, \sigma_{j,k})_\Omega| \\ & \leq \left(\frac{d}{2}\right)^{q+1} \frac{(\text{diam } \nu_{j,k})^{q+1}}{(q+1)!} \|f\|_{C^{q+1}(\nu_{j,k})} \|\boldsymbol{\omega}_{j,k}\|_1. \end{aligned}$$

Property 4) of Theorem 3.1 is crucial when it comes to feature detection. Regions where the data is smooth will lead to negligible expansion coefficients, while there is no decay with respect to the scale in regions where the data is non-smooth.

The transformation of a functional $u' \in \mathcal{X}$ into its samplet representation can be performed with linear cost using the fast samplet transform, compare [19]. We denote this basis transform in the following by

$$u' = \sum_{i=1}^N u_i \delta_{\mathbf{x}_i} = \sum_{i=1}^N [\mathbf{T}u]_i \sigma_i,$$

with a suitable linear ordering $i = i(j, k)$ of the samplets, for example a breadth-first-search-like ordering. Furthermore $\mathbf{T} \in \mathbb{R}^{N \times N}$ denotes the orthogonal samplet transformation matrix, i.e., $\mathbf{T}\mathbf{T}^\top = \mathbf{T}^\top\mathbf{T} = \mathbf{I}$.

3.2. Samplets in reproducing kernel Hilbert spaces. The samplet basis gives rise to a multiresolution basis in \mathcal{H}_X by considering the embedding

$$(8) \quad \sigma_{j,k} = \sum_{i=1}^N \omega_{j,k,i} \delta_{\mathbf{x}_i} \mapsto \psi_{j,k} = \sum_{i=1}^N \omega_{j,k,i} \mathcal{K}(\mathbf{x}_i, \cdot)$$

by means of the Riesz isometry, compare (2). Especially, for $j > 0$ there holds $\langle \psi_{j,k}, h \rangle_{\mathcal{H}} = 0$ for any $h \in \mathcal{H}$ which satisfies $h|_{\nu_{j,k}} \in \mathcal{P}_q(\nu_{j,k})$, which means that the function $\psi_{j,k}$ has vanishing moments in \mathcal{H} . Defining

$$\mathcal{W}_j := \text{span}\{\psi_{j,k}\}_k,$$

we obtain the primal multiresolution analysis

$$\mathcal{H}_X = \bigoplus_{j=0}^J \mathcal{W}_j.$$

Using the functions $\psi_{j,k}$ as ansatz- and test functions in the Galerkin formulation (5) yields the linear system

$$(9) \quad \mathbf{K}^\Sigma \boldsymbol{\beta} := \mathbf{T}\mathbf{K}\mathbf{T}^\top \boldsymbol{\beta} = \mathbf{T}\mathbf{h},$$

i.e.,

$$[\langle \psi_{j,k}, \psi_{\ell,m} \rangle_{\mathcal{H}}]_{j,k,\ell,m} = \mathbf{T}\mathbf{K}\mathbf{T}^\top$$

and

$$[\langle \psi_{j,k}, h \rangle_{\mathcal{H}}]_{j,k} = \mathbf{T}\mathbf{h}.$$

The solution of the linear system (9) is equivalent to the one of (6) by the transform

$$(10) \quad \boldsymbol{\beta} = \mathbf{T}\boldsymbol{\alpha} = \mathbf{T}\mathbf{K}^{-1}\mathbf{h}.$$

Note that a compressed version $\mathbf{K}_\varepsilon^\Sigma$ of the transformed kernel matrix \mathbf{K}^Σ can efficiently be computed by combining the compression with a hierarchical matrix approach. Indeed, if the set X is quasi-uniform, i.e., separation radius and fill-distance are of comparable size, then the matrix $\mathbf{K}_\varepsilon^\Sigma$ which is compressed with a relative compression error smaller than ε in the Frobenius norm has only $\mathcal{O}(N \log N)$ nonzero matrix entries and the cost for its computation is $\mathcal{O}(N \log N)$.

3.3. Characterization of the dual basis. Letting

$$\tilde{\omega}_{j,k} := \mathbf{K}^{-1}\omega_{j,k}, \quad \tilde{\sigma}_{j,k} := \sum_{i=1}^N \tilde{\omega}_{j,k,i} \delta_{\mathbf{x}_i},$$

the corresponding *biorthogonal (samplet) basis*, also called *dual basis*, is given by

$$\tilde{\psi}_{j,k} = \sum_{i=1}^N \tilde{\omega}_{j,k,i} \mathcal{K}(\mathbf{x}_i, \cdot).$$

The dual basis satisfies indeed

$$\begin{aligned} \langle \psi_{j,k}, \tilde{\psi}_{\ell,m} \rangle_{\mathcal{H}} &= \omega_{j,k}^{\top} \mathbf{K} \tilde{\omega}_{\ell,m} = \omega_{j,k}^{\top} \mathbf{K} \mathbf{K}^{-1} \omega_{\ell,m} \\ &= \omega_{j,k}^{\top} \omega_{\ell,m} = \delta_{j,\ell} \delta_{k,m} \end{aligned}$$

as required by the definition. Therefore, defining

$$\tilde{\mathcal{W}}_j := \text{span}\{\tilde{\psi}_{j,k}\}_k$$

yields the dual multiresolution analysis

$$\mathcal{H}_X = \bigoplus_{j=0}^J \tilde{\mathcal{W}}_j, \quad \mathcal{W}_j \perp \tilde{\mathcal{W}}_{\ell} \quad \text{for } j \neq \ell.$$

Remark 3.2. Since \mathcal{K} is particularly a Mercer kernel, see [24] for instance, it exhibits an $L^2(\Omega \times \Omega)$ -convergent spectral representation

$$\mathcal{K}(\mathbf{x}, \mathbf{y}) = \sum_i \lambda_i k_i(\mathbf{x}) k_i(\mathbf{y})$$

with $(k_i, k_j)_{L^2(\Omega)} = \delta_{i,j}$ as well as $(\hat{k}_i, \hat{k}_j)_{\mathcal{H}} = \delta_{i,j}$, where we set $\hat{k}_i := \sqrt{\lambda_i} k_i$. In the spectral basis, the primal and dual basis functions can be written as

$$\begin{aligned} \psi_{j,k} &= \sum_i (\sigma_{j,k}, \hat{k}_i)_{\Omega} \hat{k}_i \in \mathcal{H}_X, \\ \tilde{\psi}_{j,k} &= \sum_i (\tilde{\sigma}_{j,k}, \hat{k}_i)_{\Omega} \hat{k}_i \in \mathcal{H}_X \end{aligned}$$

for all $j \leq J$.

The dual basis gives rise to the representations

$$h = \sum_{i=1}^N \langle \tilde{\psi}_i, h \rangle_{\mathcal{H}} \psi_i = \sum_{i=1}^N \langle \psi_i, h \rangle_{\mathcal{H}} \tilde{\psi}_i \quad \text{for all } h \in \mathcal{H}_X.$$

Especially, employing the dual basis, the solution to (5) can directly be represented according to

$$(11) \quad s_h = \sum_{i=1}^N \beta_i \psi_i = \sum_{i=1}^N \langle \tilde{\psi}_i, h \rangle_{\mathcal{H}} \psi_i.$$

3.4. Sparse kernel interpolants. Straightforward calculation yields the identities

$$\langle \psi_{j,k}, h \rangle_{\mathcal{H}} = \omega_{j,k}^{\top} \mathbf{h}$$

and

$$\langle \tilde{\psi}_{j,k}, h \rangle_{\mathcal{H}} = \omega_{j,k}^{\top} \mathbf{K}^{-1} \mathbf{h}$$

for any $h \in \mathcal{H}$. Consequently, there holds

$$\langle \tilde{\psi}_{j,k}, h \rangle_{\mathcal{H}} = 0$$

for any $h \in \mathcal{H}_X$ which satisfies $h = \sum_{i=1}^N \alpha_i k(\mathbf{x}_i, \cdot)$ and $\alpha_i = p(\mathbf{x}_i)$, where

$$p|_{\nu_{j,k}} \in \mathcal{P}_q(\nu_{j,k}).$$

The latter means that the coefficient vector looks like a polynomial evaluated at the data sites $\mathbf{x}_i \in \nu_{j,k}$. This implies that piecewise smooth coefficient vectors amount to sparse representations with respect to the basis ψ_1, \dots, ψ_N . In addition, in view of (10), sparse coefficient vectors with respect to the basis ϕ_1, \dots, ϕ_N give rise

to sparse coefficient vectors in the basis ψ_1, \dots, ψ_N due to the locality of the samplet supports. Therefore, we conclude that sparsity in the samplet basis is the more general concept compared to the single-scale basis.

Dependent on the kernel \mathcal{K} under consideration, or the specific application, the positive definiteness assumption of the kernel matrix \mathbf{K} can numerically be violated. In such cases, a suitable regularization is required. Two common approaches, tailored to the samplet framework, are presented in the following section.

4. SCATTERED DATA APPROXIMATION

4.1. Kernel ridge regression. We first comment on the traditional kernel ridge regression. Here, one considers the squared loss function with ridge regularization in \mathcal{H} which yields the optimization problem

$$\min_{s_h \in \mathcal{H}_X} \frac{1}{2} \sum_{i=1}^N |s_h(\mathbf{x}_i) - h(\mathbf{x}_i)|^2 + \frac{\lambda}{2} \|s_h\|_{\mathcal{H}}^2.$$

This problem can be reformulated in matrix-vector form as

$$\min_{\alpha \in \mathbb{R}^N} \frac{1}{2} \|\mathbf{h} - \mathbf{K}\alpha\|_2^2 + \frac{\lambda}{2} \alpha^\top \mathbf{K}\alpha.$$

Straightforward calculation yields the first order optimality condition

$$(12) \quad (\mathbf{K} + \lambda\mathbf{I})\alpha = \mathbf{h} \quad \text{or} \quad (\mathbf{K}^\Sigma + \lambda\mathbf{I})\beta = \mathbf{T}\mathbf{h},$$

due to the unitary invariance of the euclidean norm, compare (6) and (9). The first expression computes the coefficients $\alpha \in \mathbb{R}^N$ of the kernel interpolant with respect to the single-scale basis while the second expression leads to the respective representation in samplet coordinates, i.e.,

$$s_h(\mathbf{x}) = \sum_{i=1}^N \alpha_i \mathcal{K}(\mathbf{x}, \mathbf{x}_i) = \sum_{i=1}^N \alpha_i \phi_i(\mathbf{x}) = \sum_{i=1}^N \beta_i \psi_i(\mathbf{x}),$$

compare (8). In particular, we observe that the regularization term is invariant under the samplet transform.

The smallest eigenvalue and hence the condition number of the systems in (12) is steered by the regularization parameter λ . The matrix $\mathbf{K} + \lambda\mathbf{I}$ is strictly positive definite for $\lambda > 0$ independent of the size N and, therefore, the conjugate gradient method can be used to solve the system of linear equations. The required matrix-vector multiplications can efficiently be realized in samplet coordinates. Depending on the condition number of the regularized system, the convergence might deteriorate and preconditioning becomes an issue. Diagonal scaling can be used to mitigate the ill-conditioning and seems to work in our numerical tests. However, we stress that the current samplet construction does not provide sufficient norm equivalences to render diagonal scaling a provable preconditioner. Alternatively, a (partial) sparse inverse is efficiently computable, cf. [19, 20], and can serve as an algebraic preconditioner.

4.2. Samplet basis pursuit. In this subsection, we discuss ℓ^1 -regularization which is known to promote sparsity, compare [4, 10, 12]. With regard to the basis of kernel translates, we consider the functional

$$(13) \quad \min_{\alpha \in \mathbb{R}^N} \frac{1}{2} \|\mathbf{h} - \mathbf{K}\alpha\|_2^2 + \sum_{i=1}^N w_i |\alpha_i|$$

for a given weight vector $\mathbf{w} \in \mathbb{R}^N$, see [15].

As has been argued in Subsection 3.3, a wider class of sparse solutions can be retrieved by using a samplet basis. This means that we consider

$$(14) \quad \min_{\alpha \in \mathbb{R}^N} \frac{1}{2} \|\mathbf{h} - \mathbf{K}\alpha\|_2^2 + \sum_{i=1}^N w_i |\beta_i|, \quad \text{where } \beta = \mathbf{T}\alpha.$$

In what follows, we shall refer to (14) as *samplet basis pursuit*.

We remark that, in the spirit of [8, 16], also a dictionary of multiple kernels can be employed in (13) and (14). Given kernels $\mathcal{K}_1, \dots, \mathcal{K}_L$, we are then looking for a sparse representation of the form

$$s_h = \sum_{j=1}^L \sum_{i=1}^N \alpha_i^{(j)} \mathcal{K}_j(\mathbf{x}_i, \cdot) = \sum_{j=1}^L \sum_{i=1}^N \beta_i^{(j)} \psi_i^{(j)}(\mathbf{x}),$$

compare (11). Setting

$$\mathbf{K} := [\mathbf{K}_1, \dots, \mathbf{K}_L], \quad \mathbf{K}_j := [\mathcal{K}_j(\mathbf{x}_i, \mathbf{x}_j)]_{i,j=1}^N,$$

and

$$\boldsymbol{\alpha}^\top := [\boldsymbol{\alpha}_1^\top, \dots, \boldsymbol{\alpha}_L^\top], \quad \boldsymbol{\alpha}_j \in \mathbb{R}^N,$$

this approach also amounts to (13) and (14) with the obvious modifications. The most important difference to the original problem is, of course, that the matrix \mathbf{K} is not quadratic any more which means that the underlying linear system of equations $\mathbf{K}\boldsymbol{\alpha} = \mathbf{h}$ is underdetermined.

Note that the weight vector $\mathbf{w} := [w_i]_i \in \mathbb{R}^N$ in (13) and (14), respectively, plays the role of the regularization parameter, where each coefficient is regularized individually. We refer to, e.g., [10, 25, 28] for the analysis of the regularizing properties and for appropriate parameter choice rules. Numerical algorithms to solve the optimization problems (13) and (14) are based on soft-thresholding. We recapitulate two efficient numerical realizations in the subsequent Section 5.

5. ALGORITHMS FOR SAMPLET BASIS PURSUIT

5.1. Fast iterative-shrinkage thresholding algorithm. Leveraging on the fast matrix-vector product in samplet coordinates, problem (13) can be solved by using the fast iterative shrinkage-thresholding algorithm (FISTA) from [1]. Departing from the original algorithm, two samplet transforms are applied in each step to exploit the samplet matrix compression. The resulting algorithm can be found in Algorithm 5.1. In this algorithm, and in the following ones, we use the soft-shrinkage operator

$$\text{SS}_{\mathbf{w}}(\mathbf{v}) := \text{sign}(\mathbf{v}) \max\{\mathbf{0}, |\mathbf{v}| - \mathbf{w}\},$$

where all operations have to be understood coordinate-wise.

Note that we consider here the fixed step size version, since the step size δ , which is based on the Lipschitz constant of $\mathbf{K}^\top \mathbf{K}$, can easily be computed by performing a few steps of the power iteration.

Algorithm 5.1: Fast iterative shrinkage-thresholding algorithm (FISTA)

Data: Kernel matrix $\mathbf{K}_\varepsilon^\Sigma$, data \mathbf{h}^Σ , weight \mathbf{w} , initial guess $\boldsymbol{\alpha}_0$.

Result: Coefficient vector $\boldsymbol{\alpha}$

begin

set $\boldsymbol{\gamma}_1 := \boldsymbol{\alpha}_0$, $\boldsymbol{\eta}_1 := \mathbf{T}\boldsymbol{\gamma}_1$, $t_1 = 1$
compute $\delta := 1/\ \mathbf{K}_\varepsilon^\Sigma\ _2^2$
for $i = 1, 2, \dots$ do
compute $\boldsymbol{\alpha}_k := \text{SS}_{\delta\mathbf{w}}\left(\mathbf{T}^\top(\boldsymbol{\eta}_k - \delta(\mathbf{K}_\varepsilon^\Sigma)^\top(\mathbf{K}_\varepsilon^\Sigma\boldsymbol{\eta}_k - \mathbf{h}^\Sigma))\right)$
set $t_{k+1} := \frac{1 + \sqrt{1 + 4t_k^2}}{2}$
set $\boldsymbol{\gamma}_{k+1} := \boldsymbol{\alpha}_k + \frac{t_k - 1}{t_{k+1}}(\boldsymbol{\alpha}_k - \boldsymbol{\alpha}_{k-1})$
compute $\boldsymbol{\eta}_{k+1} := \mathbf{T}\boldsymbol{\gamma}_{k+1}$

In case of problem (14), the FISTA algorithm can be employed without any modification by using samplet coordinates everywhere. We shall refer to this variant as MR-FISTA.

5.2. Semi-smooth Newton method. A particularly efficient approach for the solution of (14) is the semi-smooth Newton method, suggested in [15], which is applied to the root finding problem

$$\mathbf{0} = \boldsymbol{\beta}^* - \text{SS}_{\gamma\mathbf{w}}(\boldsymbol{\beta}^* + \gamma(\mathbf{K}^\Sigma)^\top(\mathbf{h}^\Sigma - \mathbf{K}^\Sigma\boldsymbol{\beta}^*)), \quad \gamma > 0.$$

For the reader's convenience, we recall the method in Algorithm 5.2.

If $|\mathcal{A}| = m$, the matrix $\mathbf{M}_{\mathcal{A}\mathcal{A}}$ can be formed with cost $\mathcal{O}(m^2N)$. In particular, if the active set is of moderate size, a direct solver may be employed to solve the corresponding linear system with cost $\mathcal{O}(m^3)$.

Algorithm 5.2: Multiresolution semi-smooth Newton method (MRSSN)**Data:** Kernel matrix $\mathbf{K}_\varepsilon^\Sigma$, data \mathbf{h}^Σ , weight \mathbf{w} , initial guess β_0 , parameter $\gamma > 0$, tolerance tol .**Result:** Coefficient vector β **begin**set $\beta := \beta_0$ and $\mathbf{r} := \mathcal{F}(\beta_0)$ **while** $\|\mathbf{r}\| > \text{tol}$ **do**

compute

$$\mathcal{A} := \{k \in \{1, \dots, N\} :$$

$$|[\beta + \gamma(\mathbf{K}_\varepsilon^\Sigma)^\top(\mathbf{h}^\Sigma - \mathbf{K}_\varepsilon^\Sigma\beta)]_k| > \gamma w_k\}$$

$$\mathcal{I} := \{1, \dots, N\} \setminus \mathcal{A}$$

set $\mathbf{M}_{\mathcal{A}\mathcal{A}} := \mathbf{I}_{\mathcal{A}}(\mathbf{K}_\varepsilon^\Sigma)^\top \mathbf{K}_\varepsilon^\Sigma \mathbf{I}_{\mathcal{A}}$ and $\mathbf{M}_{\mathcal{A}\mathcal{I}} := \mathbf{I}_{\mathcal{A}}(\mathbf{K}_\varepsilon^\Sigma)^\top \mathbf{K}_\varepsilon^\Sigma \mathbf{I}_{\mathcal{I}}$ solve $\gamma \mathbf{M}_{\mathcal{A}\mathcal{A}} \delta = \gamma \mathbf{M}_{\mathcal{A}\mathcal{I}} \mathbf{r} - \mathbf{I}_{\mathcal{A}} \mathbf{r}$ set $\beta := \beta + \delta$ set $\mathbf{r} := \mathcal{F}(\beta)$

Due to the local convergence of Newton's method, if the functional under consideration is numerically not strictly convex, it is favorable to iteratively decrease the regularization parameter. This procedure has been investigated earlier in [2] and is summarized in Algorithm 5.3.

Algorithm 5.3: Iteratively regularized MRSSN**Data:** Kernel matrix $\mathbf{K}_\varepsilon^\Sigma$, data \mathbf{h}^Σ , weight \mathbf{w} , initial guess β_0 , parameter $\gamma > 0$, tolerance tol .**Result:** Coefficient vector β **begin**set $\beta := \beta_0$ and choose $\mu, \mu_0 > 1$ **while** $\mu > 1$ **do**set $\beta := \text{MRSSN}(\mathbf{K}_\varepsilon^\Sigma, \mathbf{h}^\Sigma, \eta \mathbf{w}, \beta, \gamma, \text{tol})$ set $\mu := \min\{1, \mu/\mu_0\}$

6. NUMERICAL RESULTS

For the numerical experiments in Subsections 6.1 and 6.2, we consider a polynomial degree $p = 6$ for the multipole expansion and samplers with $q + 1 = 4$ vanishing moments. For the experiment in Subsection 6.3, we set $p = 4$ and $q + 1 = 3$. For the admissibility condition, we choose in all cases $\eta = d$, where d is the spatial dimension, see [19] for a definition of these parameters. Moreover, an a-posteriori compression is applied to $\mathbf{K}_\varepsilon^\Sigma$ which means that matrix entries smaller than 10^{-4} in modulus are dropped. For MRSSN, we consider throughout the numerical experiments the iteratively regularized version from Algorithm 3 and set $\mu_0 = 1.05$. The initial parameter is set to $\mu = \mu_0^{250}$, i.e., we perform 250 iterative regularization steps. Moreover, the parameter γ is estimated in a lazy fashion as the smallest eigenvalue of the matrix $\mathbf{M}_{\mathcal{A}\mathcal{A}}$, whenever the cardinality of the current active set changes by at least 2. The entailed cost is $\mathcal{O}(m^3)$, where $|\mathcal{A}| = m$, and is thus of the same order as the solution of the linear system on the active set \mathcal{A} .

All computations have been performed at the Centro Svizzero di Calcolo Scientifico (CSCS) on a single node of the Alps cluster with two AMD EPYC 7742 @2.25GHz CPUs and up to 512GB of main memory¹. For the sampler compression, up to 32 cores have been used. The sampler implementation is available online as software package FMCA² and relies on the Eigen template library³.

¹<https://www.cscs.ch/computers/alps>²<https://github.com/muchip/fmca>³<https://eigen.tuxfamily.org/>

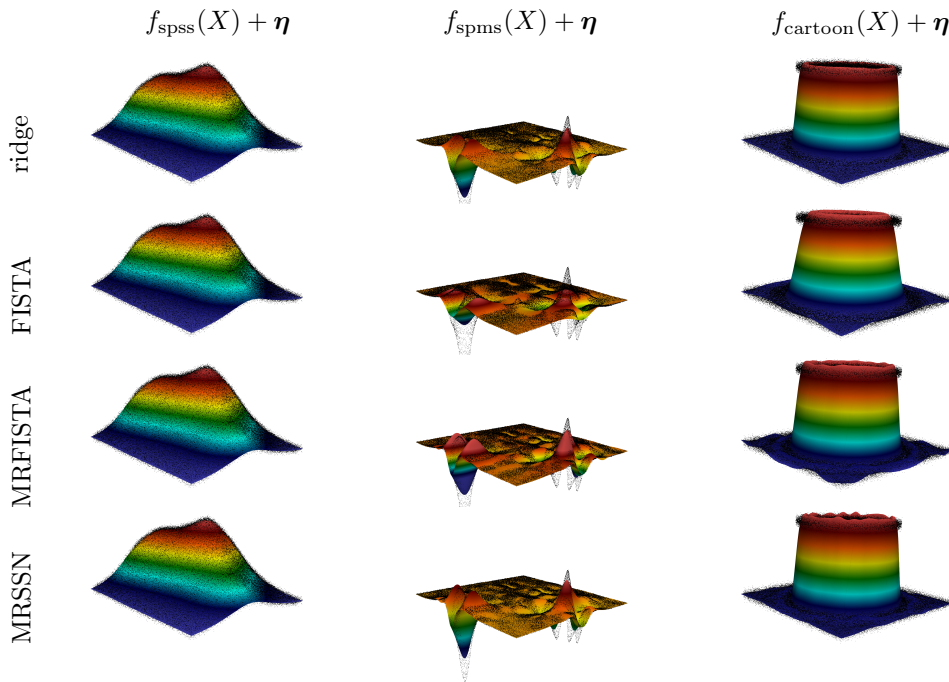


FIGURE 1. Data samples from the different data generating functions and reconstructions by the different methods.

6.1. **Benchmarks.** Given a set of uniformly distributed random points

$$X = \{\mathbf{x}_1, \dots, \mathbf{x}_N\} \subset [-0.5, 0.5]^2,$$

we consider the Matérn kernel

$$k_{3/2}(r) = \left(1 + \frac{\sqrt{3}r}{\ell\sqrt{d}}\right) e^{-\frac{\sqrt{3}r}{\ell\sqrt{d}}}$$

with correlation length given by $\ell = 0.25$. To benchmark the algorithms under consideration, we reconstruct three different data generating functions.

The first one is given by a function that has a sparse representation in the single-scale basis and is defined as

$$f_{\text{spss}}(\mathbf{x}) := c_{\text{spss}}(X) \sum_{i=1}^{10} k(\mathbf{x}_{m_i}, \mathbf{x}),$$

where $m_i \in \{1, \dots, N\}$ are randomly chosen indices.

The second function has a sparse representation in the embedded samplelet basis and reads

$$f_{\text{spms}}(\mathbf{x}) := c_{\text{spms}}(X) \sum_{i=1}^{10} \psi_{m_i}(\mathbf{x}),$$

Herein, $m_i \in \{10^3, \dots, 10^4\}$ are randomly chosen indices and the embedded samplelets $\psi_{j,k}$ are enumerated in a breadth-first-search-like ordering. This means that we randomly select functions from the low-frequency and middle-frequency part.

In both cases, the normalization constant $c(X)$ is chosen such that the respective functions attain values in $[-0.5, 0.5]$, that is

$$c(X) := \frac{1}{2 \max_{\mathbf{x} \in X} f(\mathbf{x})}.$$

Finally, we consider the cartoon function

$$f_{\text{cartoon}}(\mathbf{x}) := \begin{cases} 0.5, & \|\mathbf{x}\|_2 < 0.25, \\ 0, & \text{else,} \end{cases}$$

	ridge	FISTA	MRFISTA	MRSSN
iterations	103	10 000	10 000	411
comp. time	4.51s	1 777.42s	501.23s	58.48s
final $ \mathcal{A} $	973 731	32 963	111	101
error	$8.3 \cdot 10^{-8}$	$1.2 \cdot 10^{-2}$	$1.2 \cdot 10^{-2}$	$2.0 \cdot 10^{-9}$

TABLE 1. Results for sparse single-scale data.

	ridge	FISTA	MRFISTA	MRSSN
iterations	170	10 000	10 000	422
comp. time	11.3s	1 857.19s	506.86s	57.86
final $ \mathcal{A} $	827 864	35 194	491	163
error	$1.2 \cdot 10^{-8}$	$2.6 \cdot 10^{-2}$	$1.6 \cdot 10^{-2}$	$2.3 \cdot 10^{-7}$

TABLE 2. Results for sparse multiresolution data.

	ridge	FISTA	MRFISTA	MRSSN
iterations	118	10 000	10 000	646
comp. time	5.17s	1970.76s	607.05s	80.46s
final $ \mathcal{A} $	978 740	218 570	921	261
error	$9.6 \cdot 10^{-8}$	$7.1 \cdot 10^{-2}$	$5.6 \cdot 10^{-2}$	$3.4 \cdot 10^{-7}$

TABLE 3. Results for cartoon function data.

as an example that cannot be represented within the basis of kernel translates ϕ_1, \dots, ϕ_N , see (3).

After generating the function values, they are perturbed by additive standard gaussian noise with a noise level of 5% relative to the euclidean norm of the data. We consider $N = 10^6$ data points and the regularization parameters are set to $\lambda/N = 2 \cdot 10^{-5}$ for the ridge regression and to $w_i = 2 \cdot 10^{-5}$ for $i = 1, \dots, N$ for the ℓ^1 -regularization. The number of iterations for (MR)FISTA is limited to 10 000. Otherwise, the iteration is stopped if the gradient \mathbf{d} satisfies $\|\mathbf{d}\|_\infty < 9 \cdot 10^{-7}$. Accordingly, MRSSN is stopped if $\|\mathbf{r}\|_\infty < 9 \cdot 10^{-7}$. We remark that we choose the $\|\cdot\|_\infty$ -norm here, since it scales independently of the number of points N . The conjugate gradient method for the ridge regression is stopped with a relative tolerance of $9 \cdot 10^{-7}$. For all methods, the computation of the samplet compressed kernel matrix takes 16.04s and it contains 22 entries per row on average (upper triangular part only). The estimated relative compression error is $6.21 \cdot 10^{-5}$ in the Frobenius norm.

The obtained interpolants are evaluated on a grid with 1000×1000 points, equalling 10^6 evaluation points in total. The evaluation is performed by using the fast multipole method underlying the samplet compression with polynomial degree 4 and $\eta = 1.2$, see [19] for the details. It takes about 470s using 32 cores in all cases. The reconstructions for the different methods under consideration are depicted in Figure 1. The columns correspond to the different data generating functions, while the rows correspond to the different methods. A subsample of 10^5 data points is indicated by the black dots.

In all examples, the maximum number of iterations of (MR)FISTA was reached before the convergence criterion was met, compare Table 1, Table 2, and Table 3. The tables also show the cardinality of the final active index sets \mathcal{A} . The number for the ridge regularization is obtained counting the coefficients whose modulus is larger than the threshold as for the ℓ^1 -regularization. It can be seen that MRSSN leads throughout to the sparsest solution, while the computation time is rather moderate compared to (MR)FISTA.

A qualitative comparison of the different methods in terms of their reconstruction capabilities can be found in the visualizations in Figure 1. Except for the sparse single-scale example, FISTA performs significantly worse than the multiresolution competitors. For the sparse multiresolution example, MRSSN performs best, while the ridge regression is slightly worse. For the cartoon function, the ridge regularization provides the best tradeoff between a smooth solution and a solution which fits the data, while the results from MRFISTA and MRSSN show some oscillations at the jump.

Finally, we provide a comparison between the coefficients obtained by hard-thresholding the ridge regularized solution and the solution from MRSSN in Figure 2. The first row shows the dominant coefficients of the signal

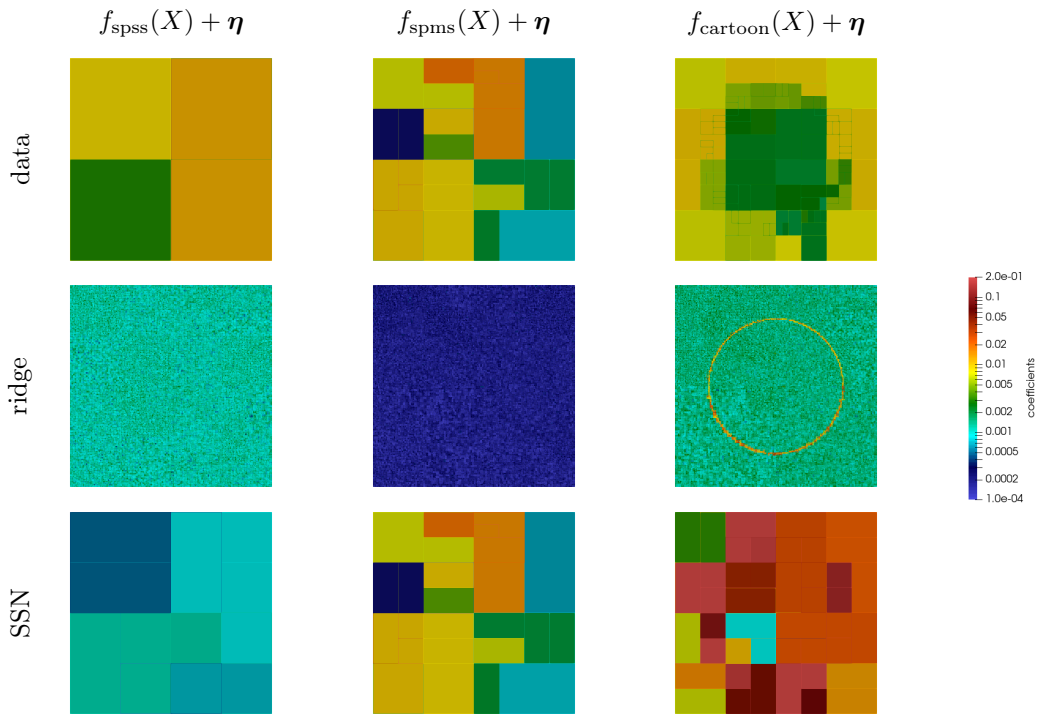


FIGURE 2. Sparsity pattern of the data (coefficients that are larger than 1% of the maximum coefficient are shown) and sparsity patterns of the corresponding solutions visualized by the supports of the active samplers in case of the ridge regression and the SSN.

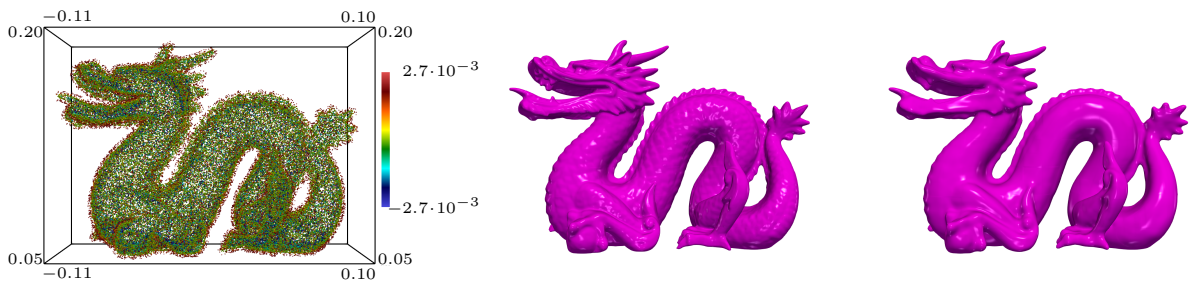


FIGURE 3. Surface reconstruction from measurements of the signed distance function. The left panel shows a subsample of the used data, the reconstruction by ridge regression is found in the middle, and the reconstruction by ℓ^1 -regularization is in the right panel.

indicated by their supports. The second row shows the coefficients obtained from the reconstruction based on ridge regularization, while the last row shows the sparse reconstruction using MRSSN. Here it can particularly be seen that the better fit of the ridge regularization for the cartoon function can be explained by the very high resolution in terms of sampler coefficients at the interface.

6.2. Surface reconstruction. In this example, we consider the reconstruction of a surface given by samples of a signed distance function, as examined earlier in [6]. We replace the greedy subsampling procedure from the aforementioned reference by imposing sparsity constraints on the coefficients of the reconstruction. As data set, we consider $5 \cdot 10^5$ randomly selected points at the surface of the Stanford dragon and $5 \cdot 10^5$ randomly selected points at a distance in $[0.002, 0.01]$ relative to the diameter of the Stanford dragon’s bounding box, compare the left panel of Figure 3, where also a subsample of 10^5 data points is shown. The total number of points is hence again $N = 10^6$.

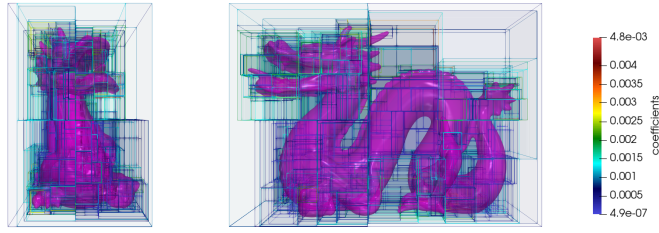


FIGURE 4. Clusters containing the active coefficients for the case of the ℓ^1 -regularization.

For the surface reconstruction, we use the exponential kernel

$$k_{\text{exp}}(r) = e^{-\frac{r}{\ell\sqrt{d}}}$$

with correlation length $\ell = 0.03$. The computation of the samplet compressed kernel matrix takes 313s and the estimated relative compression error in the Frobenius norm is $2.62 \cdot 10^{-5}$. The compressed matrix contains $1.51 \cdot 10^3$ entries per row on average (upper triangular part only). The regularization parameter is set to $\lambda/N = 5 \cdot 10^{-9}$ for the ridge regression and $w_i = 5 \cdot 10^{-9}$ for $i = 1, \dots, N$ for the ℓ^1 -regularization. The benchmark results in Subsection 6.1 suggest that MRSSN performs best. Therefore, we will exclusively rely on this algorithm in what follows. The conjugate gradient method for the ridge regression is stopped with a tolerance of $9 \cdot 10^{-7}$ while the MRSSN is stopped with $\|\mathbf{r}\|_{\infty} < 9 \cdot 10^{-7}$. The latter yields a sparse solution with only $\|\beta\|_0 = 6\,233$ non-vanishing coefficients. The conjugate gradient method takes $1.33 \cdot 10^4$ s to converge, while the MRSSN takes about four times as long with $2.02 \cdot 10^4$ s (single threaded times with parallel assembly of \mathbf{M}_{AA}).

The solution is evaluated on a structured grid with $400 \times 400 \times 400$ points, equalling $6.4 \cdot 10^7$ evaluation points. Evaluation is again performed by applying the fast multipole method and takes $2.69 \cdot 10^4$ s using 32 cores. The panel in the middle of Figure 3 shows the reconstructed surface as zero level-set of the signed distance function, and computed by the ridge regression. The sparse reconstruction is depicted in the right panel. As can clearly be seen, the sparsity constraint amounts to a smoothing of the surface. Figure 4 shows the clusters containing the active coefficients, which perfectly localize at the features of the implicit surface.

6.3. Sparse reconstruction of temperature data. In this numerical experiment, we perform the sparse reconstruction of temperature data. As dataset, we consider the monthly ERA5 temperature data set, which provides the temperature 2M above the surface. ERA5 is a reanalysis by the European Center for Medium-range Weather Forecasts (ECMWF) of global climate and weather for the past eight decades. Data is available from 1940 onwards, see [21]. We use the monthly data from 2022, which comprises 1 038 240 data points per month, resulting in 12 458 880 points in total. The original data format is World Geodesic System 1984 (WGS 84), which we transform by using the Robinson projection, compare [29], to reduce the distortion and the projection angles. From the data set we randomly select 10% of the points, resulting in $N = 1\,245\,888$ data points. The selection is performed randomly in space-time. This means that a given point in space might be present at a given time, but not at any other time. Hence, the chosen locations are not persistent in time and standard approaches like dynamic mode decomposition (DMD), see, e.g., [30] or wavelets are not directly applicable.

For the subsequent computation, the data are rescaled to the unit hyper-cube $[0, 1]^3$.

We employ two kernels,

$$\mathcal{K}_1((\mathbf{x}, t), (\mathbf{y}, t')) := k_{3/2}(\|\mathbf{x} - \mathbf{y}\|_2)k_{\text{per}}(|t - t'|)$$

and

$$\mathcal{K}_2(\mathbf{z}, \mathbf{z}') := k_{\text{exp}}(\|\mathbf{z} - \mathbf{z}'\|_2), \quad \mathbf{z} := (\mathbf{x}, t), \quad \mathbf{z}' := (\mathbf{y}, t'),$$

where we set the corresponding components according to

$$\begin{aligned} k_{3/2}(r) &:= (1 + 5\sqrt{3})e^{-5\sqrt{3}r}, \\ k_{\text{per}}(r) &:= e^{-50 \sin^2(\pi r)}, \\ k_{\text{exp}}(r) &:= e^{-100r}. \end{aligned}$$

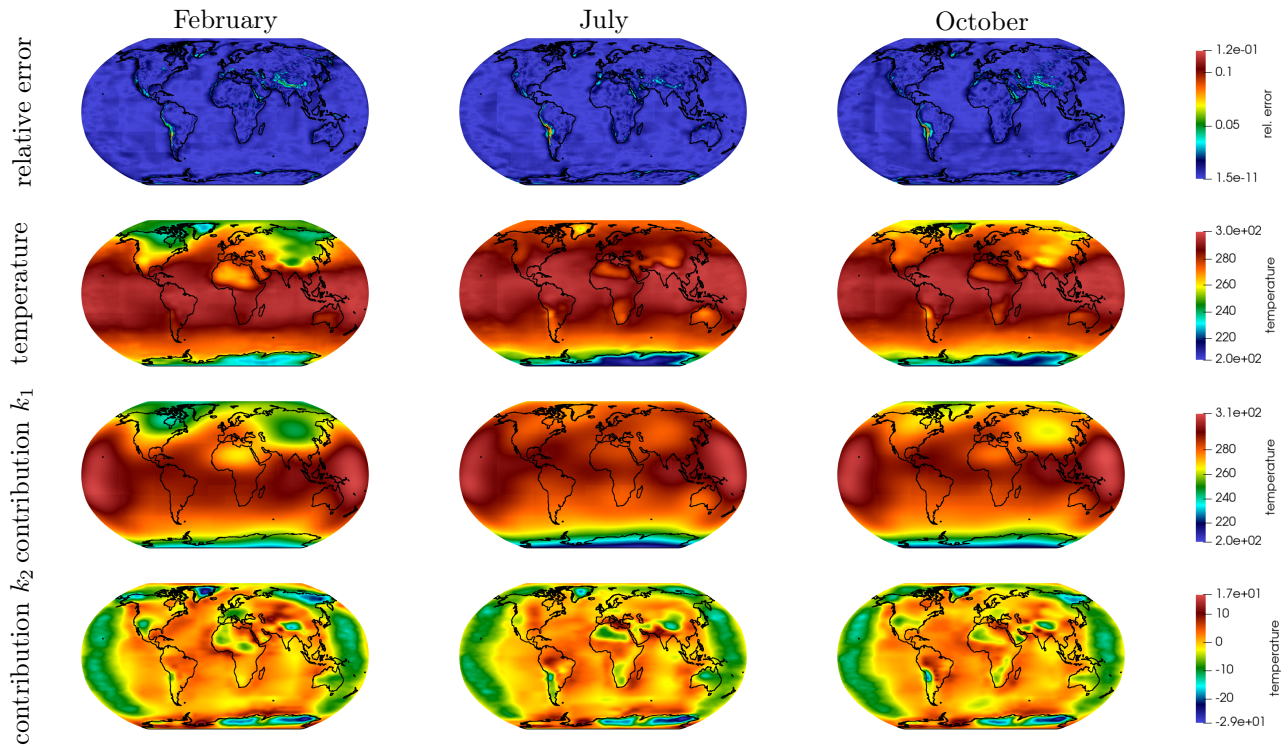


FIGURE 5. Sparse reconstruction of temperature data using two kernels. The relative error is shown in the top row, the reconstructed temperature in the second row, the contribution of k_1 is seen in the third row and the contribution of k_2 in the last row.

The kernel \mathcal{K}_1 is a tensor product kernel comprised of a Matérn-3/2 kernel in space and a periodic kernel in time, both with relatively large correlation lengths. This kernel is intended to capture the smooth parts of the temperature distribution over time. The second kernel \mathcal{K}_2 is a very rough exponential kernel in space time and intended to capture sharp features. The overall time for the compression of both kernels is 508s. The compressed matrix contains for \mathcal{K}_1 contains 507 entries per row on average and the estimated relative compression error is $6.02 \cdot 10^{-5}$ in the Frobenius norm. The compressed matrix contains for \mathcal{K}_2 contains 939 entries per row on average and the estimated relative compression error is $3.37 \cdot 10^{-4}$ in the Frobenius norm. We set $w_i = 5 \cdot 10^{-9}$ for $i = 1, \dots, N$ and MRSSN is stopped if $\|\mathbf{r}\|_\infty < 9 \cdot 10^{-7}$. The evaluation of the interpolant at all 12 458 880 points of the full data set approximately takes between 50s and 73s per time step using 32 cores.

The top row of Figure 5 shows the reconstruction error evaluated at the full data set for the months February, July, and October. The relative error is everywhere smaller than 12% and strongly localized at the mountains (Andes and Himalayas). The second row shows the reconstructed temperature distribution evaluated at the full data set. The third row shows the contribution of \mathcal{K}_1 , where $\|\alpha_1\|_0 = 712$. The kernel \mathcal{K}_1 indeed perfectly captures the coarse-scale structure of the temperature distribution. The last row shows the contribution of \mathcal{K}_2 , where $\|\alpha_2\|_0 = 5430$. This kernel localizes coast lines and mountains and thus actually captures the sharp features. Moreover, it accounts for the periodicity in longitudinal direction.

We finally remark that it would also be possible to directly work with the temperature data mapped to the earth's surface, which would however come at the cost of a four dimensional approach instead of a three dimensional one.

7. CONCLUSION

In this article, we have presented the novel concept of samplet basis pursuit. Samplets constitute a multiresolution basis tailored to scattered data. This renders them the method of choice for feature detection and sparse reconstruction of such data. Interpolation is directly facilitated by embedding of samplets into the reproducing

kernel Hilbert space context. An efficient computational algorithm for the computation of sparse representations is obtained by employing the multiresolution semi-smooth Newton method in samplet coordinates. Besides a benchmark problem, we have presented extensive numerical studies for the reconstruction of implicit surfaces from measurements of the signed distance function and for the reconstruction of temperature data from scattered measurements. In particular, samplelets naturally allow for the approximation of scattered data in space-time and are therefore also able to capture dynamic features.

ACKNOWLEDGEMENTS

DB was funded by the Swiss Federal Office of Energy SFOE as part of the SWEET project SURE. HH was funded in parts by the SNSF by the grant “Adaptive Boundary Element Methods Using Anisotropic Wavelets” (200021_192041). MM was funded in parts by the SNSF starting grant “Multiresolution methods for unstructured data” (TMSGI2_211684).

REFERENCES

- [1] A. Beck and M. Teboulle. A fast iterative shrinkage-thresholding algorithm for linear inverse problems. *SIAM J. Imaging Sci.*, 2(1):183–202, 2009.
- [2] B. Blaschke, A. Neubauer, and O. Scherzer. On convergence rates for the iteratively regularized gauss-newton method. *IMA J. Numer. Anal.*, 17(3):421–436, 1997.
- [3] S. Boyd, N. Parikh, E. Chu, B. Peleato, and J. Eckstein. Distributed optimization and statistical learning via the alternating direction method of multipliers. *Found. Trends Mach. Learn.*, 3(1):1–122, 2010.
- [4] E. Candès, J. Romberg, and T. Tao. Stable signal recovery from incomplete and inaccurate measurements. *Comm. Pure Appl. Math.*, 59(8):1207–1223, 2006.
- [5] E.J. Candès and D.L. Donoho. Curvelets: A surprisingly effective nonadaptive representation for objects with edges. In A. Cohen, C. Rabut, and L. Schumaker, editors, *Curves and Surface Fitting: Saint-Malo 1999*, page 105–120, Nashville, 2000. Vanderbilt University Press.
- [6] J.C. Carr, R.K. Beatson, J.B. Cherrie, T.J. Mitchell, W.R. Fright, B.C. McCallum, and T.R. Evans. Reconstruction and representation of 3D objects with radial basis functions. In *Proceedings of the 28th annual conference on Computer graphics and interactive techniques*, SIGGRAPH '01, pages 67–76, New York, 2001. Association for Computing Machinery.
- [7] S. Chen and D.L. Donoho. Basis pursuit. In *Proceedings of 1994 28th Asilomar Conference on Signals, Systems and Computers*, volume 1, pages 41–44, Pacific Grove, CA, USA, 1994. IEEE.
- [8] S.S. Chen, D.L. Donoho, and M.A. Saunders. Atomic decomposition by basis pursuit. *SIAM J. Sci. Comput.*, 20(1):33–61, 1998.
- [9] X. Chen, Z. Nashed, and L. Qi. Smoothing methods and semismooth methods for nondifferentiable operator equations. *SIAM J. Numer. Anal.*, 38(4):1200–1216, 2000.
- [10] I. Daubechies, M. Defrise, and C. De Mol. An iterative thresholding algorithm for linear inverse problems with a sparsity constraint. *Comm. Pure Appl. Math.*, 57:1413–1457, 2004.
- [11] M.N. Do and M. Vetterli. The contourlet transform: an efficient directional multiresolution image representation. *IEEE Trans. Image Proc.*, 14:2091–2106, 2005.
- [12] D.L. Donoho. Compressed sensing. *IEEE Trans. Inf. Theory*, 52(4):1289–1306, 2006.
- [13] G.E. Fasshauer. *Meshfree approximation methods with MATLAB*. World Scientific, River Edge, 2007.
- [14] S. Foucart and H. Rauhut. *A Mathematical Introduction to Compressive Sensing*. Applied and Numerical Harmonic Analysis. Birkhäuser, New York, 2013.
- [15] R. Griesse and D.A. Lorenz. A semismooth Newton method for Tikhonov functionals with sparsity constraints. *Inverse Problems*, 24(3):035007, 2008.
- [16] V. Guigue, A. Rakotomamonjy, and S. Canu. Kernel basis pursuit. In J. Gama, R. Camacho, P. B. Brazdil, A. M. Jorge, and L. Torgo, editors, *Machine Learning: ECML 2005*, pages 146–157, Berlin, Heidelberg, 2005. Springer.
- [17] K. Guo and D. Labate. Optimally sparse multidimensional representation using shearlets. *SIAM J. Math. Anal.*, 39(1):298–318, 2007.
- [18] H. Harbrecht, U. Kähler, and R. Schneider. Wavelet Galerkin BEM on unstructured meshes. *Comput. Vis. Sci.*, 8(3–4):189–199, 2005.
- [19] H. Harbrecht and M. Multerer. Samplelets: Construction and scattered data compression. *J. Comput. Phys.*, 471:111616, 2022.
- [20] H. Harbrecht, M. Multerer, O. Schenk, and C. Schwab. Multiresolution kernel matrix algebra. *arXiv-Preprint*, arXiv:2211.11681, 2022.
- [21] H. Hersbach, B. Bell, P. Berrisford, S. Hirahara, A. Horányi, J. Muñoz-Sabater, J. Nicolas, C. Peubey, R. Radu, D. Schepers, A. Simmons, C. Soci, S. Abdalla, X. Abellan, G. Balsamo, P. Bechtold, G. Biavati, J. Bidlot, M. Bonavita, G. De Chiara, P. Dahlgren, D. Dee, M. Diamantakis, R. Dragani, J. Flemming, R. Forbes, M. Fuentes, A. Geer, L. Haimberger, S. Healy, R. J. Hogan, E. Hólm, M. Janisková, S. Keeley, P. Laloyaux, P. Lopez, C. Lupu, G. Radnoti, P. de Rosnay, I. Rozum, F. Vamborg, S. Villaume, and J.-N. Thépaut. The era5 global reanalysis. *Q. J. R. Meteorol.*, 146(730):1999–2049, 2020.

- [22] M. Hintermüller, K. Ito, and K. Kunisch. The primal-dual active set strategy as a semismooth Newton method. *SIAM J. Optim.*, 13:865–888, 2003.
- [23] G. James, D. Witten, T. Hastie, and R. Tibshirani. *An Introduction to Statistical Learning*. Springer Texts in Statistics. Springer, New York, 2013.
- [24] H. König. *Eigenvalue distribution of compact operators*, volume 16 of *Operator Theory: Advances and Applications*. Birkhäuser, Basel, 1986.
- [25] D.A. Lorenz. Convergence rates and source conditions for tikhonov regularization with sparsity constraints. *J. Inverse Ill-Posed Probl.*, 16(5):463–478, 2008.
- [26] S.G. Mallat and W.L. Hwang. Singularity detection and processing with wavelets. *IEEE Trans. Inf. Theory*, 38(2):617–643, 1992.
- [27] S.G. Mallat and Z. Zhang. Matching pursuits with time-frequency dictionaries. *IEEE Trans. Sign. Proc.*, 41(12):3397–3415, 1993.
- [28] R. Ramlau and G. Teschke. A Tikhonov-based projection iteration for nonlinear ill-posed problems with sparsity constraints. *Numer. Math.*, 104(2):177–203, 2006.
- [29] A.H. Robinson. A new map projection: Its development and characteristics. *International yearbook of cartography*, 14(1974):145–155, 1974.
- [30] P. J. Schmid. Dynamic mode decomposition of numerical and experimental data. *J. Fluid Mech.*, 656:5–28, 2010.
- [31] T. Tao and E.J. Candès. Near-optimal signal recovery from random projections: universal encoding strategies? *IEEE Trans. Inf. Theory*, 52(12):5406–5425, 2006.
- [32] J. Tausch and J. White. Multiscale bases for the sparse representation of boundary integral operators on complex geometry. *SIAM J. Sci. Comput.*, 24(5):1610–1629, 2003.
- [33] J.A. Tropp. Greed is good: algorithmic results for sparse approximation. *IEEE Trans. Inf. Theory*, 50(10):2231–2242, 2004.
- [34] H. Wendland. *Scattered Data Approximation*. Cambridge University Press, Cambridge, 2004.

DAVIDE BAROLI, ISTITUTO EULERO, UNIVERSITÀ DELLA SVIZZERA ITALIANA, LUGANO, VIA LA SANTA 1, 6962 LUGANO, SVIZZERA.

Email address: michael.multerer@usi.ch

HELMUT HARBRECHT, DEPARTEMENT FÜR MATHEMATIK UND INFORMATIK, UNIVERSITÄT BASEL, SPIEGELGASSE 1, 4051 BASEL, SWITZERLAND.

Email address: helmut.harbrecht@unibas.ch

MICHAEL MULTERER, ISTITUTO EULERO, UNIVERSITÀ DELLA SVIZZERA ITALIANA, VIA LA SANTA 1, 6962 LUGANO, SVIZZERA.

Email address: michael.multerer@usi.ch